I&EC research
Industrial & Engineering Chemistry Research
pubs.acs.org/IECR
Article

Synthesis of Guanidinium-Based Poly(ionic liquids) with Nonporosity for Highly Efficient SO_2 Capture from Flue Gas

Fei-Feng Mao, Yan Zhou, Wenshuai Zhu, Xiao-Yan Sang, Zhang-Min Li, and Duan-Jian Tao*

Cite This: *Ind. Eng. Chem. Res.* 2021, 60, 5984−5991

ABSTRACT: Because of considerable adsorption capacities of competitive gases N_2 and CO_2, many kinds of porous materials suffer from unsatisfied SO_2/CO_2 and SO_2/N_2 selectivities and thus hardly achieve deep removal of SO_2 from flue gas. Herein, a novel type of guanidinium-based poly(ionic liquid) with the feature of nonporosity was designed and prepared through a facile copolymerization procedure. It is very attractive that nonporous guanidinium-based poly(ionic liquids) P([allyl-TMG]Br-DVB) by polymerization of (allyl-tetramethylguanidine)-bromide with divinylbenzene had almost excluded the adsorption of N_2 (0.01 mmol g^{-1}) and CO_2 (0.07 mmol g^{-1}) but showed very high SO_2 capacity (9.79 mmol g^{-1}) at 25 °C and 1 bar. The high selectivities of SO_2/CO_2 (452) and SO_2/N_2 (2294) were accordingly obtained. Furthermore, column breakthrough experiments confirmed the excellent separation performance of P([allyl-TMG]Br-DVB) in deeply eliminating 2000 ppm SO_2 in the mixture of $SO_2/N_2/CO_2$. The employment of nonporous poly(ionic liquids) as efficient adsorbents is an effective strategy for the deep removal of SO_2 from flue gas.

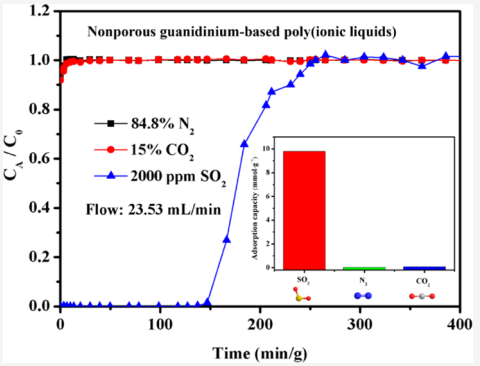

INTRODUCTION

Nowadays, sulfur dioxide (SO_2) emitted from burning low-grade fossil fuels has attracted worldwide attention because of its great threat to human health and environmental quality. The SO_2 content in flue gases is usually in the range of 500−3000 ppm, and over 95% SO_2 can be captured and removed by traditional amine solutions or limestone slurry.[1,2] However, these conventional flue gas desulfurization (FGD) technologies have several inherent drawbacks such as hard deep removal of SO_2, easy-to-scaling and wearing, amine degradation, and equipment corrosion. Thus, the design and development of new separation materials for efficient and selective capture of SO_2 are highly conceived and constantly demanded.

Until now, a variety of porous materials, such as porous carbon,[3−5] porous organic polymer,[6] and metal−organic frameworks (MOFs),[7−9] have been designed and developed for efficient adsorption of various gases including SO_2, CO_2, CH_4, H_2, etc.[10−12] However, it should be noted that SO_2 is usually along with various competitive gases such as N_2 and CO_2.[13] The abundant pores in porous materials also can enhance the interaction between the adsorbents and competitive gas molecules. As a result, many porous materials exhibited considerable adsorption capacities for CO_2 and N_2, significantly reducing the selectivities of SO_2/CO_2 and SO_2/N_2.[14] For this reason, it is interesting and worth designing novel adsorbent materials for SO_2 capture, which exhibit high SO_2 uptake capacity but almost exclude the adsorption of CO_2 and N_2.

Recently, ionic liquids (ILs) have been popularly considered as novel and efficient solvents for gas absorption because of their excellent ability for selective molecular recognition.[15,16] So far, a lot of ILs have been reported and used for efficient capture of SO_2 and CO.[17−20] For example, Xing et al.[21] prepared a kind of nonporous imidazolium-based poly(ionic liquid) xerogel, which showed large SO_2 adsorption capacity (7.78 mmol g^{-1}) and high selectivity of SO_2/CO_2 (up to 614) via a swelling mechanism but excluded the adsorption of CO_2 and N_2. However, such nonporous poly(ionic liquids) need a complex preparation process involving microfluidic technology and photopolymerization, and the column breakthrough performance is also not satisfied entirely. Considering the inadequate research on nonporous poly(ionic liquids) for SO_2 capture, it is very promising and rationally conceived to facilely synthesize other nonporous poly(ionic liquids) for efficient adsorption of SO_2 with excellent breakthrough performance.

Herein, we designed and prepared a new type of guanidinium-based poly(ionic liquid) through a facile one-pot process involving the formation of guanidinium ILs and subsequent copolymerization of guanidinium ILs with divinylbenzene (Scheme 1). Systematic characterizations manifested that these kinds of guanidinium-based poly(ionic liquids) showed the feature of a nonporosity structure. More

Received: March 22, 2021
Accepted: April 5, 2021
Published: April 14, 2021

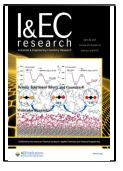

Scheme 1. One-Pot Procedure of Guanidinium-Based Poly(ionic liquids)

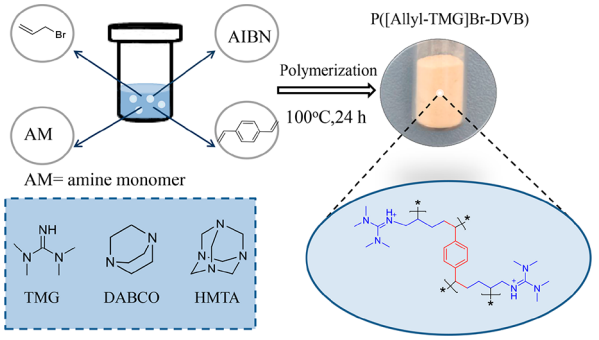

importantly, guanidinium-based poly(ionic liquids) could be employed as superior adsorbents for highly efficient SO_2 capture. In addition, their excellent performance for deep elimination of 2000 ppm SO_2 in the mixture of $SO_2/N_2/CO_2$ was further confirmed via column breakthrough experiments at 25 °C and 1 bar.

EXPERIMENTAL SECTION

Materials. Tetramethylguanidine (TMG, 99%), 2,2′-azobis(2-methylpropionitrile) (AIBN, 98%), divinylbenzene (DVB, 80%), hexamethylenetetramine (HMTA, 99%), triethylenediamine (DABCO, 98%), and 3-bromopropene (98%) were purchased from Shanghai Macklin Biochemical Co. Ltd. CO_2 (99.999%), N_2 (99.999%), and SO_2 (99.99%) were provided by Jiangxi Huate Special Gas Co. Ltd. All of the other chemicals were used as received without further purification.

Preparation of Guanidinium-Based Poly(ionic liquids). As shown in Scheme 1, guanidinium-based poly(ionic liquids) were prepared through a facile one-pot process involving the preparation of guanidinium ILs and radical copolymerization of guanidinium ILs with divinylbenzene. In a typical run, 3-bromopropene (1.21 g, 10 mmol) was added dropwise to an ethyl acetate solution (10 mL) of TMG (1.15 g, 10 mmol). Then, DVB (1.30 g, 10 mmol) was added to the mixture and stirred at 60 °C for 12 h. After that, guanidinium IL [allyl-TMG]Br was generated, which agrees with our previous work on CO_2 adsorption and utilization.[22] Subsequently, AIBN (0.05 g) and H_2O (2.5 mL) were further charged to the mixture and stirred at 100 °C for 24 h. After the reaction, the solid powder was washed with tetrahydrofuran and deionized water five times. Finally, a white solid powder labeled as P([allyl-TMG]Br-DVB) was obtained after drying in a vacuum oven at 80 °C for 12 h.

For comparison, the other two kinds of tertiary amine-based poly(ionic liquids) were prepared, but with the replacement of TMG with HMTA and DABCO, respectively, that is, polymerization of (allyl-hexamethylenetetramine)bromide or (allyl-triethylenediamine)bromide with DVB. These two polymers were then labeled as P([allyl-HMTA]Br-DVB) and P([allyl-DABCO]Br-DVB).

Characterizations. The crystallographic structures of samples were detected using a Rigaku RINT-2200 X-ray diffractometer (XRD) using Cu Kα radiation (40 kV, 20 mA). Fourier transform infrared (FTIR) spectra were collected on a NEXUS870 FTIR spectrometer. Thermogravimetric analysis (TGA) was carried out on a PerkinElmer Diamond instrument with a heating rate of 10 °C/min under a nitrogen atmosphere. The morphologies and sizes of samples were analyzed by scanning electron microscopy (SEM, HITACHI SU8020) and transmission electron microscopy (TEM, JEOL JEM-2100) in high resolution. The nitrogen adsorption/desorption analysis was recorded on a Micromeritics TriStar II 3020 instrument at 77 K, and the surface area was calculated using the Brunauer–Emmett–Teller (BET) method. The X-ray photoelectron spectroscopy (XPS) spectra were obtained on a Kratos AXIS SUPRA with Al Kα radiation.

Adsorption Measurements. The schematic for adsorption of SO_2 is shown in Figure S1 in the Supporting Information, which is the same as our previous work.[20] The SO_2 adsorption capacity was measured and calculated by a dual-chamber volumetric method. More details can be found in the Supporting Information. Three duplicate experiments were run for each sample to obtain averaged values of SO_2 adsorption. For the recycle test, SO_2-loaded poly(ionic liquids) were heated to 80 °C for desorbing SO_2 under a vacuum of 0.1 kPa for 2 h. The regenerated poly(ionic liquids) were employed for the next adsorption of SO_2. Furthermore, the adsorption isotherms of CO_2 and N_2 at 25 °C by poly(ionic liquids) were determined on Micromeritics TriStar II 3020 apparatus.

Breakthrough Tests. The breakthrough tests were measured on homemade apparatus for removal of 2000 ppm SO_2 at 25 °C and 1 bar (Figure S2, Supporting Information). In the dynamic separation experiment, P([allyl-TMG]Br-DVB) samples (0.35 g) were packed into a Φ 6.3 × 140 mm stainless steel column and the column was activated under reduced pressure at 120 °C for 2 h. A carrier gas (He ≥ 99.999%) was used to purge the adsorption bed for about 4 h at room temperature. Then, the mixed gas composed of 2000 ppm SO_2, 84.8% N_2, and 15% CO_2 was passed at a flow rate of 23.53 mL min^{-1} for the adsorption of SO_2. The gas flows were controlled at the inlet by a mass flow meter, and gas chromatography (Agilent HP7890B) continuously monitored the effluent gas from the adsorption bed.

RESULTS AND DISCUSSION

Characterization of Poly(ionic liquids). Figure 1 shows the FTIR spectra of three kinds of poly(ionic liquids) for identification of their chemical groups. It is demonstrated that all of these poly(ionic liquid) samples showed typical stretching vibration peaks around 1450–1610 cm^{-1}, corre-

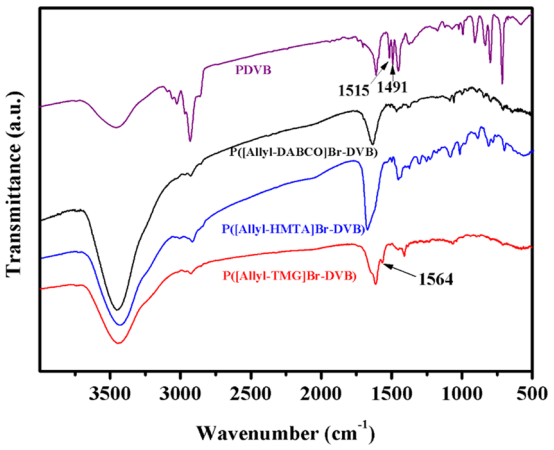

Figure 1. FTIR spectra of P([allyl-TMG]Br-DVB), P([allyl-HMTA]-Br-DVB), and P([allyl-DABCO]Br-DVB).

https://doi.org/10.1021/acs.iecr.1c01118
Ind. Eng. Chem. Res. 2021, 60, 5984–5991

sponding to the skeletal benzene ring of DVB.[23,24] This finding indicates the successful copolymerization of TMG with DVB. Moreover, the poly(ionic liquid) P([allyl-TMG]Br-DVB) exhibited the bending vibration of the N−H group at 1564 cm^{-1},[25] but the other two IL poly(ionic liquids) P([allyl-HMTA]Br-DVB) and P([allyl-DABCO]Br-DVB) did not. Subsequently, XRD was used to measure the crystal microstructures of these poly(ionic liquids). It can be seen from Figure S3 that no crystalline phase was detected and the broadened peak at around 2θ = 22° was assigned to the patterns of amorphous carbons in these poly(ionic liquids). In addition, the thermal stability of P([allyl-TMG]Br-DVB), P([allyl-HMTA]Br-DVB), and P([allyl-DABCO]Br-DVB) samples was further investigated (Figure S4, Supporting Information). It is obvious that the initial decomposition temperature of P([allyl-TMG]Br-DVB) was as high as 260 °C and was superior to the other two poly(ionic liquids), showing excellent thermal stability of P([allyl-TMG]Br-DVB).

The porosities of P([allyl-TMG]Br-DVB), P([allyl-HMTA]-Br-DVB), and P([allyl-DABCO]Br-DVB) were further characterized by N_2 adsorption/desorption analysis. As shown in Figure 2, it is observed that the poly(ionic liquids) P([allyl-

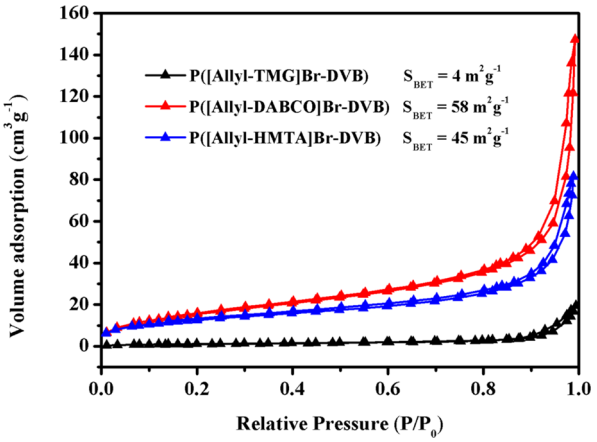

Figure 2. N_2 adsorption/desorption of P([allyl-TMG]Br-DVB), P([allyl-HMTA]Br-DVB), and P([allyl-DABCO]Br-DVB).

HMTA]Br-DVB) and P([allyl-DABCO]Br-DVB) had a type-II isotherm with an H3 hysteresis loop. Most of the N_2 uptake occurred at 0.9−1.0 P/P_0, indicating the presence of slit-shaped pores.[26] Then, the surface areas of P([allyl-HMTA]Br-DVB) and P([allyl-DABCO]Br-DVB) were calculated to be 58 and 45 $m^2\ g^{-1}$, respectively. In contrast, the isotherm of the P([allyl-TMG]Br-DVB) sample showed extremely low N_2 uptake capacity, and its surface area was only 4 $m^2\ g^{-1}$, demonstrating the nonporosity of P([allyl-TMG]Br-DVB). This demonstrates that compared with the monomers HMTA and DABCO, the absence of a ring-shaped structure in the TMG monomer can result in nonporous P([allyl-TMG]Br-DVB) with a very low surface area.

Figure 3 shows the SEM and TEM images of P([allyl-TMG]Br-DVB) and P([allyl-HMTA]Br-DVB), respectively. It is revealed that the primary particles of nonporous poly(ionic liquid) P([allyl-TMG]Br-DVB) interconnected with each other to form a very dense framework. In contrast, the particles of P([allyl-HMTA]Br-DVB) did not aggregate seriously. A randomly oriented but more loose structure was observed for the poly(ionic liquid) P([allyl-HMTA]Br-DVB),

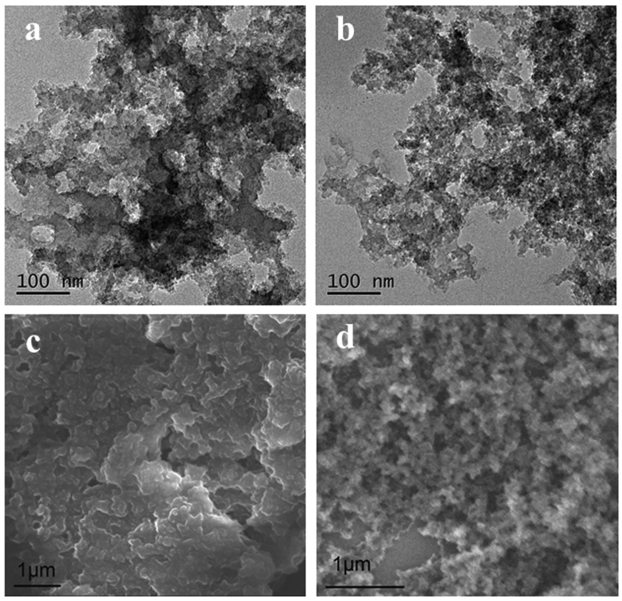

Figure 3. TEM images of (a) P([allyl-TMG]Br-DVB) and (b) P([allyl-HMTA]Br-DVB) and SEM images of (c) P([allyl-TMG]Br-DVB) and (d) P([allyl-HMTA]Br-DVB).

as well as the nonporous feature of P([allyl-TMG]Br-DVB) was confirmed by the TEM images. To gain an insight into the chemical states of C, N, O, and Br species in P([allyl-TMG]Br-DVB), P([allyl-HMTA]Br-DVB), and P([allyl-DABCO]Br-DVB), XPS characterization was further performed, as shown in Figure 4. It is demonstrated that the C, N, O, and Br elements were detected in the full-scan spectra of these three poly(ionic liquids) samples (Figure S5, Supporting Information). Moreover, the N 1s XPS spectra of P([allyl-TMG]Br-DVB) and P([allyl-HMTA]Br-DVB) can be deconvoluted to two types of nitrogen species, corresponding to pyrrolic N at 400.0 eV and quaternary N at 401.2 eV[27,28] (Figure 4a). Also, the binding energy of quaternary N in P([allyl-DABCO]Br-DVB) was observed at 402.4 eV. These results confirm that the fragments of guanidinium ILs and ammonium ILs were formed and existed in these three poly(ionic liquids). In addition, in the bromide region (Figure 4b), the binding energies at around 67 and 68 eV were attributed to Br $3d_{5/2}$ and Br $3d_{3/2}$, respectively.[19,22] It is worth noting that the binding energy of Br 3d in P([allyl-TMG]Br-DVB) was found to be slightly lower than in the cases of P([allyl-HMTA]Br-DVB) and P([allyl-DABCO]Br-DVB). The monomer guanidinium IL in P([allyl-TMG]Br-DVB) may have an electron-donating effect on the bromide ion, and thereby enhance the electron density of Br^-, resulting in the relatively low binding energy of Br 3d in P([allyl-TMG]Br-DVB).

SO_2 Adsorption Performance. The adsorption capacity of SO_2 on three poly(ionic liquids), P([allyl-TMG]Br-DVB), P([allyl-HMTA]Br-DVB), and P([allyl-DABCO]Br-DVB), was measured at 25 °C and 1 bar to assess their SO_2 capture ability. As shown in Figure 5, these three poly(ionic liquids) exhibited different SO_2 adsorption capacities, and the sequence was P([allyl-TMG]Br-DVB) > P([allyl-DABCO]Br-DVB) > P([allyl-HMTA]Br-DVB). Nonporous poly(ionic liquid) P-([allyl-TMG]Br-DVB) showed the highest SO_2 uptake capacity of 9.79 mmol/g at 25 °C and 1 bar. As mentioned above, P([allyl-TMG]Br-DVB) owned the lower Br 3d binding energy compared with P([allyl-HMTA]Br-DVB) and P([allyl-

https://doi.org/10.1021/acs.iecr.1c01118
Ind. Eng. Chem. Res. 2021, 60, 5984−5991

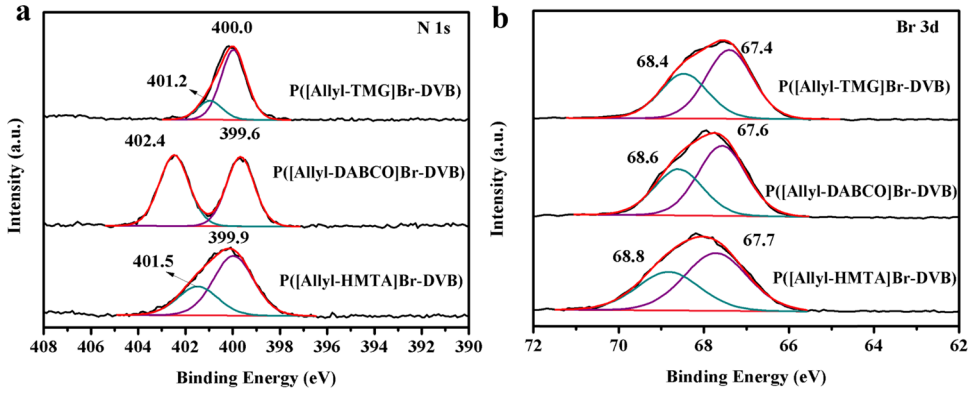

Figure 4. XPS N 1s (a) and Br 3d (b) spectra of P([allyl-TMG]Br-DVB), P([allyl-HMTA]Br-DVB), and P([allyl-DABCO]Br-DVB).

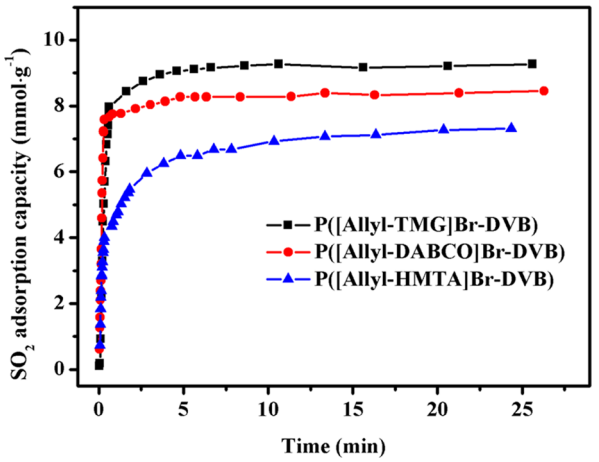

Figure 5. SO_2 adsorption rate for P([allyl-TMG]Br-DVB), P([allyl-HMTA]Br-DVB), and P([allyl-DABCO]Br-DVB) at 25 °C and 1 bar.

DABCO]Br-DVB), indicating that the Br^- ion in P([allyl-TMG]Br-DVB) has a more negative charge and exhibits a relatively strong Lewis basicity. Thus, P([allyl-TMG]Br-DVB) showed a better SO_2 affinity and resulted in a higher SO_2 uptake capacity. Moreover, the effect of adsorption temperature on the performance of P([allyl-TMG]Br-DVB) was also studied (Figure S6, Supporting Information). It is showed that the SO_2 uptake capacity decreased obviously with increasing temperature, indicating an exothermic adsorption process. Although the absorption temperature was as high as 333 K, the SO_2 uptake still reached 3.5 mmol g^{-1}. The isosteric heats of SO_2 adsorption on P([allyl-TMG]Br-DVB) were found to be from −55 to −45 kJ mol^{-1} (Figure S7, Supporting Information).

More importantly, nonporous poly(ionic liquid) P([allyl-TMG]Br-DVB) exhibited a very fast SO_2 adsorption rate with a saturation time of around 5 min. A SO_2 uptake capacity of 8 mmol/g could be achieved by P([allyl-TMG]Br-DVB) at a very short time of 0.5 min. This unprecedented SO_2 adsorption rate is significantly superior to the performance of nonporous ionic xerogels and many porous materials including zeolites,[29,30] porous carbons,[3,5] covalent organic polymers,[31,32] and MOFs.[7−9] In addition, the interaction between P([allyl-TMG]Br-DVB) and SO_2 was further characterized by FTIR spectroscopy (Figure 6). For the SO_2-loaded P([allyl-TMG]-Br-DVB) sample, the stretching vibration peak intensity of the −NH group decreased significantly (Figure 6a), as well as two new peaks at 1120 and 1290 cm^{-1} were observed and assigned to the symmetric and asymmetrical vibration of S═O, respectively (Figure 6b).[33−36] These results confirm the chemical interaction between SO_2 and P([allyl-TMG]Br-DVB), in which the adsorption binding site is the −NH moiety on P([allyl-TMG]Br-DVB).

It is known that the competitive gases N_2 and CO_2 often coexist with SO_2 in the most flue gas.[37] A high adsorption selectivity for removal of SO_2 is very necessary for an FGD process. Thus, the adsorption isotherms of N_2 and CO_2 on the poly(ionic liquids), P([allyl-TMG]Br-DVB), P([allyl-HMTA]-Br-DVB), and P([allyl-DABCO]Br-DVB) were further measured at 25 °C and 1 bar (Figures 7and S8, Supporting

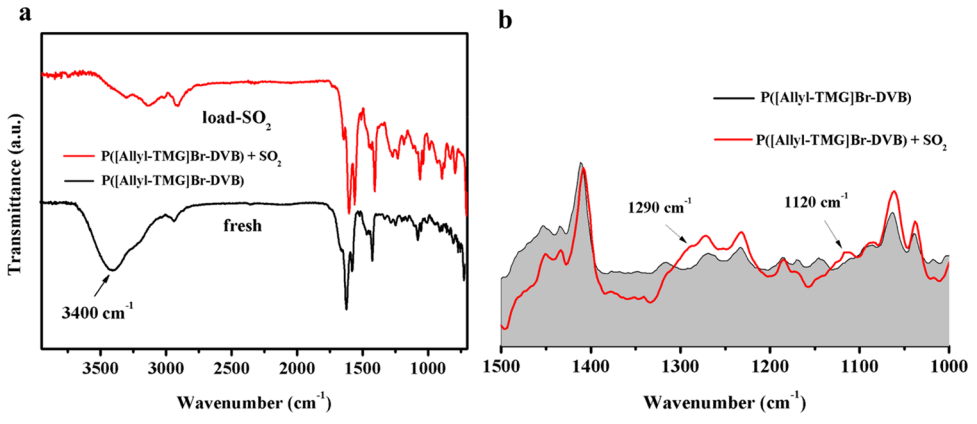

Figure 6. Comparison of FTIR spectra of fresh P([allyl-TMG]Br-DVB) and P([allyl-TMG]Br-DVB) + SO_2.

https://doi.org/10.1021/acs.iecr.1c01118
Ind. Eng. Chem. Res. 2021, 60, 5984−5991

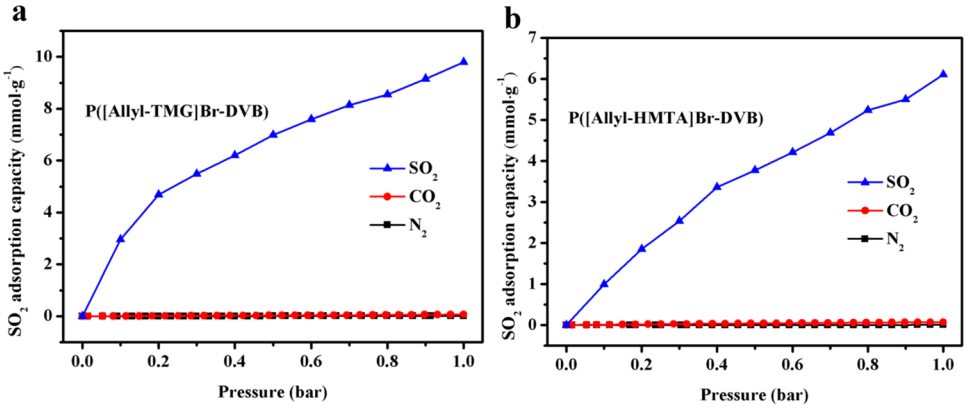

Figure 7. SO_2, CO_2, and N_2 adsorption on (a) P([allyl-TMG]Br-DVB) and (b) P([allyl-HMTA]Br-DVB) at 25 °C and 1 bar.

Table 1. Adsorption Capacity of SO_2, CO_2, and N_2 on Three Poly(ionic liquids) and Other Adsorbents at 25 °C and 1 bar

	SO_2 (mmol g^{-1})		CO_2 (mmol g^{-1})	N_2 (mmol g^{-1})			
samples	0.1 bar	1 bar	1 bar	1 bar	SO_2/CO_2 (10/90)	SO_2/N_2 (10/90)	ref
P([allyl-TMG]Br-DVB)	2.95	9.79	0.07	0.01	452	2294	this work
P([allyl-DABCO]Br-DVB)	2.36	7.69	0.13	0.02	181	2062	this work
P([allyl-HMTA]Br-DVB)	0.99	6.10	0.07	0.01	131	871	this work
MFM-300(In)	7.20	8.28	3.61	0.25	50	2700	40
SIFSIX-1-Cu	8.70	11.00	4.94	0.29	71	3146	14
SIFSIX-3-Zn	1.89	2.10	2.65		7	507	14
MFM-305-CH3	4.38	5.16	2.39	0.35	17	136	9
Ni(bdc)(ted)0.5	3.50	9.97	2.27				41
HNIP	3.54	7.20	0.37	0.01	91	3186	20

Information). The impact of their porosities and surface areas on SO_2/N_2 and SO_2/CO_2 adsorption selectivities were further evaluated. The results demonstrated that the highly dense structure of nonporous P([allyl-TMG]Br-DVB) successfully excluded the adsorption of N_2 and CO_2. The N_2 and CO_2 adsorption capacities were then as low as 0.01 and 0.07 mmol g^{-1}, respectively. As a result, a high SO_2/CO_2 selectivity (452) for the SO_2/CO_2 (10/90, v/v) mixture and outstanding SO_2/N_2 selectivity (2294) for the SO_2/N_2 (10/90, v/v) mixture was achieved at 25 °C and 1 bar, respectively (Table 1). On the contrary, the poly(ionic liquid) P([allyl-DABCO]Br-DVB) with a relatively large surface area displayed more N_2 and CO_2 adsorption capacities, which results in unsatisfied SO_2/N_2 and SO_2/CO_2 adsorption selectivities. Therefore, P([allyl-TMG]-Br-DVB) has a good potential for highly selective trace SO_2 capture in the FGD process.

To confirm the actual SO_2/CO_2 and SO_2/N_2 separation performance on nonporous poly(ionic liquid) P([allyl-TMG]-Br-DVB), experimental breakthrough tests were carried out with a simulated flue gas mixture containing 2000 ppm SO_2 with a flow rate of 23.53 mL min^{-1} at 25 °C and 1 bar (Figures 8 and S9, Supporting Information). It is found that compared with porous P([allyl-HMTA]Br-DVB), the breakthrough time of SO_2 on nonporous P([allyl-TMG]Br-DVB) could reach up to 150 min g^{-1}. This means that highly efficient and deep elimination of SO_2 could be achieved with clean N_2 and CO_2 eluted from the bed by nonporous poly(ionic liquid) P([allyl-TMG]Br-DVB). Furthermore, P([allyl-TMG]Br-DVB) was treated in the saturated steam at 80 °C for 24 h to test its water stability. It is found that the breakthrough performance of steam-treated P([allyl-TMG]Br-DVB) for 2000 ppm SO_2 did not reduce obviously, and the retention time was retained at ~150 min g^{-1} (Figure S10, Supporting Information).

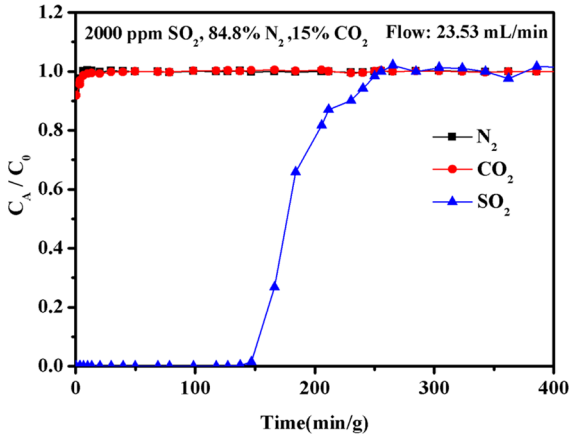

Figure 8. Experimental column breakthrough curves for $SO_2/N_2/CO_2$ (2000 ppm SO_2) separation with P([allyl-TMG]Br-DVB) at 25 °C and 1 bar.

Comparison of Poly(ionic liquids) with other Adsorbents in the Literature. The adsorption amount ratio of SO_2 and CO_2 on different adsorbent materials at a pressure of 0.5 bar was summarized and is shown in Figure 9. It is noted that P([allyl-TMG]Br-DVB) exhibited the highest SO_2/CO_2 uptake ratio among most materials including MOFs, zeolites, porous organic polymers, and active carbons.[9,29,38−41] Moreover, we also compared the SO_2 adsorption capability of nonporous poly(ionic liquids) with other adsorbents reported in the previous literature (Table 1). It is indicated that the SO_2 capability of nonporous P([allyl-TMG]Br-DVB) is comparable

https://doi.org/10.1021/acs.iecr.1c01118
Ind. Eng. Chem. Res. 2021, 60, 5984−5991

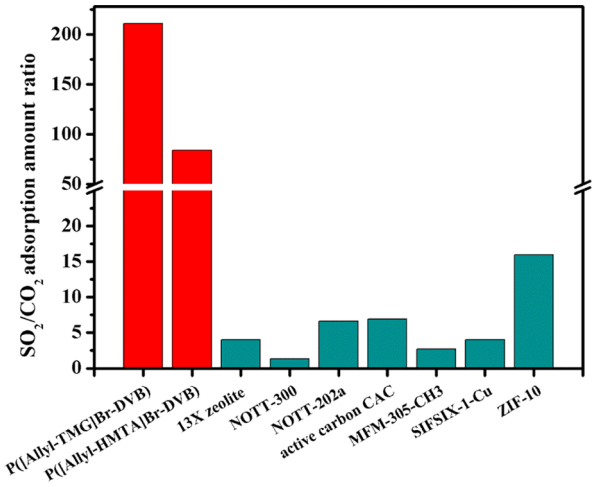

Figure 9. Comparison of the adsorption amount ratio of SO_2 and CO_2 at 0.5 bar. (1) P([allyl-TMG]Br-DVB) at 25 °C; (2) P([allyl-HMTA]Br-DVB) at 25 °C; (3) 13X zeolite at 323 K; (4) NOTT-300 at 0 °C; (5) NOTT-202a at 0 °C; (6) activated carbon CAC at 25 °C; (7) MFM-305-CH3 at 25 °C; (8) MOF material SIFSIX-1-Cu at 25 °C; and (9) MOF material ZIF-10 at 25 °C.

to the benchmarking MOF adsorbents MFM-300(In),[40] SIFSIX-1-Cu, and Ni(bdc)(ted)0.5.[41] More importantly, the N_2 and CO_2 capacities of nonporous P([allyl-TMG]Br-DVB) are extremely low, which are significantly less than those of many reported porous materials. Therefore, it is well accepted that the nonporous characteristic of P([allyl-TMG]Br-DVB) is in favor of highly efficient and selective SO_2 adsorption and shows good potential in the FGD process.

Recycling Test of P([allyl-TMG]Br-DVB). Recycling performance related to the process cost is important for potential applications. Six cycles of SO_2 adsorption and desorption by nonporous P([allyl-TMG]Br-DVB) were performed to test the reversibility of nonporous P([allyl-TMG]Br-DVB). As shown in Figure 10a, nonporous P([allyl-TMG]Br-DVB) still kept initial SO_2 uptake performance after the sixth run. Moreover, FTIR spectroscopy was performed to evaluate the completion of SO_2 desorption. Compared with fresh P([allyl-TMG]Br-DVB), the recycled P([allyl-TMG]Br-DVB) had no obvious changes in the characteristic peaks of FTIR spectra (Figure 10b), implying the total desorption of SO_2. All of these results suggest that nonporous P([allyl-TMG]Br-DVB) has a good enough reversibility to run SO_2 adsorption and desorption cycles.

CONCLUSIONS

In summary, a kind of guanidinium poly(ionic liquid) was prepared and used for highly efficient SO_2 capture. It is demonstrated that guanidinium poly(ionic liquid) P([allyl-TMG]Br-DVB) with the nature of nonporosity had almost excluded N_2 and CO_2 uptake but exhibited very high SO_2 capacity at 25 °C and 1 bar. Accordingly, the highest selectivity of SO_2/CO_2 and SO_2/N_2 was up to 452 and 2294 (i.e., 10/90 mixture at 25 °C and 1 bar), respectively. Furthermore, the excellent separation performance for eliminating 2000 ppm SO_2 on P([allyl-TMG]Br-DVB) was examined and verified by the breakthrough experiments with the mixture of $SO_2/CO_2/N_2$. In addition, P([allyl-TMG]Br-DVB) showed good structural stability and enough reversibility to run SO_2 adsorption/desorption during six cycles. It is believed that nonporous poly(ionic liquids) show good potential for the actual flue gas desulfurization process.

ASSOCIATED CONTENT

Supporting Information

The Supporting Information is available free of charge at https://pubs.acs.org/doi/10.1021/acs.iecr.1c01118.

Apparatus for the determination of gas adsorption (Figure S1); breakthrough experiment apparatus (Figure S2); XRD patterns (Figure S3); TGA curves (Figure S4); XPS wide spectra (Figure S5); the effect of adsorption temperature on SO_2 (Figure S6); isosteric heats of SO_2 adsorption (Figure S7); SO_2, CO_2, and N_2 adsorption (Figure S8); experimental column breakthrough curves for SO_2/N_2 (Figure S9); and experimental column breakthrough curves for $SO_2/N_2/CO_2$ (Figure S10) (PDF)

AUTHOR INFORMATION

Corresponding Author

Duan-Jian Tao − *College of Chemistry and Chemical Engineering, Jiangxi Normal University, Nanchang 330022, China;* orcid.org/0000-0002-8835-0341; Email: djtao@jxnu.edu.cn

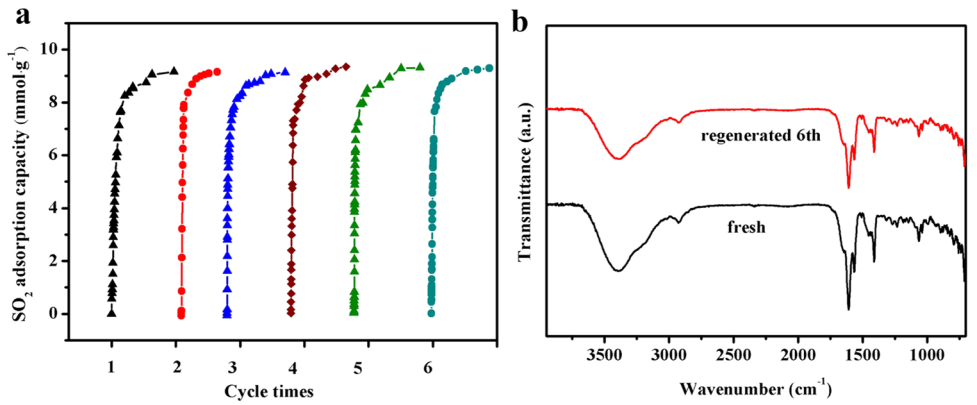

Figure 10. (a) Six cycles of SO_2 adsorption and desorption by P([allyl-TMG]Br-DVB). (b) FTIR spectra of fresh and regenerated P([allyl-TMG]Br-DVB).

https://doi.org/10.1021/acs.iecr.1c01118
Ind. Eng. Chem. Res. 2021, 60, 5984−5991

Authors

Fei-Feng Mao − *College of Chemistry and Chemical Engineering, Jiangxi Normal University, Nanchang 330022, China*

Yan Zhou − *College of Chemistry and Chemical Engineering, Jiangxi Normal University, Nanchang 330022, China*

Wenshuai Zhu − *School of Chemistry and Chemical Engineering, Institute for Energy Research, Jiangsu University, Zhenjiang 212013, China;* orcid.org/0000-0003-1265-4709

Xiao-Yan Sang − *College of Chemistry and Chemical Engineering, Jiangxi Normal University, Nanchang 330022, China*

Zhang-Min Li − *College of Chemistry and Chemical Engineering, Jiangxi Normal University, Nanchang 330022, China*

Complete contact information is available at: https://pubs.acs.org/10.1021/acs.iecr.1c01118

Notes

The authors declare no competing financial interest.

■ ACKNOWLEDGMENTS

This work was financially supported by the National Natural Science Foundation of China (21566011 and 22068013), the Natural Science Foundation of Jiangxi Province (20192ACBL20025), and the Key Research and Development Program of Jiangxi Province (20202BBGL73118).

■ REFERENCES

(1) Cui, L.; Lu, J. W.; Song, X. D.; Tang, L. S.; Li, Y. Z.; Dong, Y. Energy conservation and efficiency improvement by coupling wet flue gas desulfurization with condensation desulfurization. *Fuel* **2021**, *285*, No. 119209.

(2) Huang, R. T.; Wu, H.; Yang, L. J. Investigation on condensable particulate matter emission characteristics in wet ammonia-based desulfurization system. *J. Environ. Sci.* **2020**, *92*, 95−105.

(3) Rosas, J. M.; Ruiz Rosas, R.; Rodríguez Mirasol, J.; Cordero, T. Kinetic study of SO_2 removal over lignin-based activated carbon. *Chem. Eng. J.* **2017**, *307*, 707−721.

(4) Zhang, J. Y.; Zhang, J. B.; Li, M. J.; Wu, Z. L.; Dai, S.; Huang, K. Solvent-free and one-pot synthesis of ultramicroporous carbons with ultrahigh nitrogen contents for sulfur dioxide capture. *Chem. Eng. J.* **2020**, *391*, No. 123579.

(5) Wang, A.; Fan, R. Q.; Pi, X. X.; Hao, S.; Zheng, X. B.; Yang, Y. L. N-Doped porous carbon derived by direct carbonization of metal−organic complexes crystal materials for SO_2 adsorption. *Cryst. Growth Des.* **2019**, *19*, 1973−1984.

(6) Zhang, P. F.; Chen, D.; Chen, N. Q.; Huang, K.; Tao, D. J.; Li, M. J.; Dai, S. Synthesis of porous sulfonamide polymers by capturing atmospheric sulfur dioxide. *ChemSusChem* **2018**, *11*, 1751−1755.

(7) Chen, K. J.; Scott, H. S.; Madden, D. G.; Pham, T.; Kumar, A.; Bajpai, A.; Lusi, M.; Forrest, K. A.; Space, B.; Perry, J. J.; Zaworotko, M. J. Benchmark C_2H_2/CO_2 and CO_2/C_2H_2 separation by two closely related hybrid ultramicroporous materials. *Chem* **2016**, *1*, 753−765.

(8) Brandt, P.; Nuhnen, A.; Lange, M.; Möllmer, J.; Weingart, O.; Janiak, C. Metal−organic frameworks with potential application for SO_2 separation and flue gas desulfurization. *ACS Appl. Mater. Interfaces* **2019**, *11*, 17350−17358.

(9) Li, L.; Da silva, I.; Kolokolov, D. I.; Han, X.; Li, J. N.; Smith, G.; Cheng, Y. Q.; Daemen, L. L.; Morris, C. G.; Godfrey, H. G. W.; Jacques, N. M.; Zhang, X. R.; Manuel, P.; Frogley, M. D.; Murray, C. A.; Ramirez-Cuesta, A. J.; Cinque, G.; Tang, C. C.; Stepanov, A. G.; Yang, S. H.; Schroder, M. Post-synthetic modulation of the charge distribution in a metal−organic framework for optimal binding of carbon dioxide and sulfur dioxide. *Chem. Sci.* **2019**, *10*, 1472−1482.

(10) Liu, L. B.; Chen, H. B.; Shiko, E.; Fan, X. F.; Zhou, Y. F.; Zhang, G.; Luo, X.; Hu, X. Y. Eric. Low-cost DETA impregnation of acid-activated sepiolite for CO_2 capture. *Chem. Eng. J.* **2018**, *353*, 940−948.

(11) Hu, X. Y. Eric.; Liu, L. B.; Luo, X.; Xiao, G. K.; Shiko, E.; Zhang, R.; Fan, X. F.; Zhou, Y. F.; Liu, Y.; Zeng, Z. G.; Li, C. E. A review of N-functionalized solid adsorbents for post-combustion CO_2 capture. *Appl. Energy* **2020**, *260*, No. 114244.

(12) Gao, S. Q.; Zhang, P. L.; Wang, Z. Z.; Cui, G. K.; Qiu, J. K.; Wang, J. J. Ionic liquid functionalized 3D mesoporous FDU-12 for effective SO_2 capture. *ACS Sustainable Chem. Eng.* **2020**, *8*, 586−593.

(13) Zhang, S. G.; Zhang, J. H.; Zhang, Y.; Deng, Y. Q. Nanoconfined ionic liquids. *Chem. Rev.* **2017**, *117*, 6755−6833.

(14) Cui, X. L.; Yang, Q. W.; Yang, L. F.; Krishna, R.; Zhang, Z. G.; Bao, Z. B.; Wu, H.; Ren, Q. L.; Zhou, W.; Chen, B. L.; Xing, H. B. Ultrahigh and selective SO_2 uptake in inorganic anion-pillared hybrid porous materials. *Adv. Mater.* **2017**, *29*, No. 1606929.

(15) Choudhary, H.; Pernak, J.; Shamshina, J. L.; Niemczak, M.; Giszter, R.; Chrzanowski, Ł.; Praczyk, T.; Marcinkowska, K.; Cojocaru, O. A.; Rogers, R. D. Two herbicides in a single compound: double salt herbicidal ionic liquids exemplified with glyphosate, dicamba, and MCPA. *ACS Sustainable Chem. Eng.* **2017**, *5*, 6261−6273.

(16) Tao, D. J.; Chen, F. F.; Tian, Z. Q.; Huang, K.; Mahurin, S. M.; Jiang, D.; Dai, S. Highly efficient carbon monoxide capture by carbanion-functionalized ionic liquids through C-site interactions. *Angew. Chem., Int. Ed.* **2017**, *56*, 6843−6847.

(17) Tao, D. J.; Qu, F.; Li, Z. M.; Zhou, Y. Promoted absorption of CO at high temperature by cuprous-based ternary deep eutectic solvents. *AIChE J.* **2021**, *67*, No. e17106.

(18) Suo, X.; Yu, Y.; Qian, S. H.; Zhou, L.; Cui, X. L.; Xing, H. B. Tailoring the pore size and chemistry of ionic ultramicroporous polymers for trace sulfur dioxide capture with high capacity and selectivity. *Angew. Chem.* **2021**, *133*, 7062−7067.

(19) Qi, Y. F.; Hu, X. D.; Liu, Y. Z.; Sun, D. S.; Li, R. H.; Zhu, H. T. Highly efficient and reversible absorption of SO_2 by hydroxyl ammonium ionic liquids at low partial pressure. *J. Chem. Technol. Biotechnol.* **2019**, *94*, 3325−3332.

(20) An, X. C.; Li, Z. M.; Zhou, Y.; Zhu, W. S.; Tao, D. J. Rapid capture and efficient removal of low-concentration SO_2 in simulated flue gas by hypercrosslinked hollow nanotube ionic polymers. *Chem. Eng. J.* **2020**, *394*, No. 124859.

(21) Xia, L.; Cui, Q.; Suo, X.; Li, Y. H.; Cui, X. L.; Yang, Q. W.; Xu, J. H.; Yang, Y. W.; Xing, H. B. Efficient, selective, and reversible SO_2 capture with highly crosslinked ionic microgels via a selective swelling mechanism. *Adv. Funct. Mater.* **2018**, *28*, No. 1704292.

(22) Hui, W.; He, X. M.; Xu, X. Y.; Chen, Y. M.; Zhou, Y.; Li, Z. M.; Zhang, L. Q.; Tao, D. J. Highly efficient cycloaddition of diluted and waste CO_2 into cyclic carbonates catalyzed by porous ionic copolymers. *J. CO_2 Util.* **2020**, *36*, 169−176.

(23) Fu, R. Q.; Woo, J. J.; Seo, S. J.; Lee, J. S.; Moon, S. H. Sulfonated polystyrene/polyvinyl chloride composite membranes for PEMFC applications. *J. Membr. Sci.* **2008**, *309*, 156−164.

(24) Guo, Z. J.; Jiang, Q. W.; Shi, Y. M.; Li, J.; Yang, X. N.; Hou, W.; Zhou, Y.; Wang, J. Tethering dual hydroxyls into mesoporous poly(ionic liquid)s for chemical fixation of CO_2 at ambient conditions: a combined experimental and theoretical study. *ACS Catal.* **2017**, *7*, 6770−6780.

(25) Cota, I.; Chimentao, R.; Sueiras, J.; Medina, F. The DBU-H_2O complex as a new catalyst for aldol condensation reactions. *Catal. Commun.* **2008**, *9*, 2090−2094.

(26) Qiu, Y. L.; Xing, Z. P.; Guo, M. J.; Zhao, T. Y.; Wang, Y.; Chen, P.; Li, Z. Z.; Pan, K.; Zhou, W. Cadmium sulfide quantum dots/dodecahedral polyoxometalates/oxygen-doped mesoporous graphite carbon nitride with Z-scheme and Type-II as tandem heterojunctions for boosting visible-light-driven photocatalytic performance. *J. Colloid Interface Sci.* **2021**, *582*, 752−763.

(27) Fang, R.; Luque, R.; Li, Y. W. Selective aerobic oxidation of biomass-derived HMF to 2,5-diformylfuran using a MOF-derived magnetic hollow Fe−Co nanocatalyst. *Green Chem.* **2016**, *18*, 3152−3157.
(28) Liu, F. J.; Wang, L.; Sun, Q.; Zhu, L. F.; Meng, X. J.; Xiao, F. S. Transesterification catalyzed by ionic liquids on superhydrophobic mesoporous polymers: heterogeneous catalysts that are faster than homogeneous catalysts. *J. Am. Chem. Soc.* **2012**, *134*, 16948−16950.
(29) Deng, H.; Yi, H. H.; Tang, X. L.; Yu, Q. F.; Ning, P.; Yang, L. P. Adsorption equilibrium for sulfur dioxide, nitric oxide, carbon dioxide, nitrogen on 13X and 5A zeolites. *Chem. Eng. J.* **2012**, *188*, 77−85.
(30) Yi, H. H.; Deng, H.; Tang, X. L.; Yu, Q. F.; Zhou, X.; Liu, H. Y. Adsorption equilibrium and kinetics for SO_2, NO, CO_2 on zeolites FAU and LTA. *J. Hazard. Mater.* **2012**, *203*−*204*, 111−117.
(31) Fu, Y.; Wang, Z. Q.; Li, S. Z.; He, X. M.; Pan, C. Y.; Yan, J.; Yu, G. P. Functionalized covalent triazine frameworks for effective CO_2 and SO_2 removal. *ACS Appl. Mater. Interfaces* **2018**, *10*, 36002−36009.
(32) Lee, G. Y.; Lee, J.; Vo, H. T.; Kim, S.; Lee, H.; Park, T. Amine-functionalized covalent organic framework for efficient SO_2 capture with high reversibility. *Sci. Rep.* **2017**, *7*, No. 557.
(33) Li, X. S.; Zhang, L. Q.; Zheng, Y.; Zheng, C. G. Effect of SO_2 on CO_2 absorption in flue gas by ionic liquid 1-ethyl-3-methylimidazolium acetate. *Ind. Eng. Chem. Res.* **2015**, *54*, 8569−8578.
(34) Yang, S. H.; Liu, L. F.; Sun, J. L.; Thomas, K. M.; Davies, A. J.; George, M. W.; Blake, A. J.; Hill, A. H.; Fitch, A. N.; Tang, C. C.; Schröder, M. Irreversible network transformation in a dynamic porous host catalyzed by sulfur dioxide. *J. Am. Chem. Soc.* **2013**, *135*, 4954−4957.
(35) Cui, G. K.; Lin, W. J.; Ding, F.; Luo, X. Y.; He, X.; Li, H. R.; Wang, C. M. Highly efficient SO_2 capture by phenyl-containing azole-based ionic liquids through multiple-site interactions. *Green Chem.* **2014**, *16*, 1211−1216.
(36) Yang, Z. Z.; He, L. N.; Song, Q. W.; Chen, K. H.; Liu, A. H.; Liu, X. M. Highly efficient SO_2 absorption/activation and subsequent utilization by polyethylene glycol-functionalized Lewis basic ionic liquids. *Phys. Chem. Chem. Phys.* **2012**, *14*, 15832−15839.
(37) Yi, H. H.; Wang, Z. X.; Liu, H. Y.; Tang, X. L.; Ma, D.; Zhao, S. Z.; Zhang, B. W.; Gao, F. Y.; Zuo, Y. R. Adsorption of SO_2, NO, and CO_2 on activated carbons: equilibrium and thermodynamics. *J. Chem. Eng. Data* **2014**, *59*, 1556−1563.
(38) Ding, L. F.; Yazaydin, A. O. The effect of SO_2 on CO_2 capture in zeolitic imidazolate frameworks. *Phys. Chem. Chem. Phys.* **2013**, *15*, 11856−11861.
(39) Yang, S. H.; Sun, J. L.; Ramirez-Cuesta, A. J.; Callear, S. K.; David, W. I. F.; Anderson, D. P.; Newby, R.; Blake, A. J.; Parker, J. E.; Tang, C. C.; Schröder, M. Selectivity and direct visualization of carbon dioxide and sulfur dioxide in a decorated porous host. *Nat. Chem.* **2012**, *4*, 887−894.
(40) Savage, M.; Cheng, Y. Q.; Easun, T. L.; Eyley, J. E.; Argent, S. P.; Warren, M. R.; Lewis, W.; Murray, C.; Tang, C. C.; Frogley, M. D.; Cinque, G.; Sun, J. L.; Rudić, S.; Murden, R. T.; Benham, M. J.; Fitch, A. N.; Blake, A. J.; Ramirez-Cuesta, A. J.; Yang, S.; Schröder, M. Selective adsorption of sulfur dioxide in a robust metal-organic framework material. *Adv. Mater.* **2016**, *28*, 8705−8711.
(41) Tan, K.; Canepa, P.; Gong, Q. H.; Liu, J.; Johnson, D. H.; Dyevoich, A.; Thallapally, P. K.; Thonhauser, T.; Li, J.; Chabal, Y. J. Mechanism of preferential adsorption of SO_2 into two microporous paddle wheel frameworks $M(bdc)(ted)_{0.5}$. *Chem. Mater.* **2013**, *25*, 4653−4662.

https://doi.org/10.1021/acs.iecr.1c01118
Ind. Eng. Chem. Res. 2021, 60, 5984−5991